Experimental and theoretical analysis of particle size effect in liquid-phase hydrogenation of diphenylacetylene

Markov, Pavel V.; Mashkovsky, Igor S.; Bragina, Galina O.; Wärnå, Johan; Bukhtiyarov, Valerii I.; Stakheev, Alexander Yu; Murzin, Dmitry Yu

Published in:
Chemical Engineering Journal

DOI:
10.1016/j.cej.2020.126409

Published: 15/01/2021

Document Version
Accepted author manuscript

EXPERIMENTAL AND THEORETICAL ANALYSIS OF PARTICLE SIZE EFFECT IN LIQUID-PHASE HYDROGENATION OF DIPHENYLACETYLENE

Pavel V. Markov[1], Igor S. Mashkovsky[1], Galina O. Bragina[1], Johan Wärnå[2], Valerii I. Bukhtiyarov[3], Alexandr Yu.Stakheev[1], Dmitry Yu. Murzin[2*]

[1]N.D. Zelinsky Institute of Organic Chemistry RAS, Moscow, Russia

[2]Process Chemistry Centre, Åbo Akademi University, Turku, Finland

[3]Boreskov Institute of Catalysis SB RAS, Novosibirsk, Russia

*dmurzin@abo.fi

ABSTRACT

The liquid-phase hydrogenation of diphenylacetylene (DPA) over 1 wt.% Pd/Al_2O_3 catalysts with the mean palladium cluster size varying from 1.9 to 20 nm was studied at 5 bar H_2 pressure and 25°C. Hydrogenation of the triple bond was found to be structure sensitive and turnover frequency increased as Pd cluster size increased, while TOF in hydrogenation of the intermediate stilbene was essentially independent on the cluster size. Selectivity to stilbene was rather high (90-94%) and tends to increase with an increasing of Pd particle size.

A reaction network was proposed for diphenylacetylene hydrogenation involving formation of *cis*- and *trans*- stilbene and their subsequent hydrogenation. The effect of Pd nanoparticle size on the hydrogenation kinetics was analyzed and discussed using a geometric approach based on the respective contribution of low (edges, corners) and highly coordinated sites (terraces) for a cubooctahedral shape of metal clusters. A quantitative description of the concentration dependences was performed incorporating the Pd particle size in the rate equations through changes in dispersion and the ratio of sites of different coordination. An excellent correspondence between theory and experiments was demonstrated.

Key-words: structure sensitivity, hydrogenation of diphenylacetylene, palladium, kinetic modelling

INTRODUCTION

Selective hydrogenation of alkynes is of significant importance for industry and laboratory practice for synthesis of bulk and fine chemicals [1]. Hydrogenation of acetylenic compounds to ethylenic ones is widely applied in manufacturing of polymers [2, 3]. Ethylene fraction after steam cracking usually contains significant amounts of acetylene as impurity. Presence of acetylene in the ethylene feed leads to irreversible poisoning of metallocene polymerization catalysts, because acetylene strongly adsorbs on the catalyst active sites and blocks the polymerization process [4]. Additionally, acetylene admixture can deteriorate the properties of the final polymers [5, 6]. Therefore, the acetylene concentration in the ethylene feed should be reduced below 3-5 ppm. Selective hydrogenation of acetylene to ethylene avoiding over hydrogenation to ethane is the most effective way to purify the ethylene containing feeds to meet stringent requirements of polymer-grade purity. Another industrially important reaction is selective hydrogenation of phenylacetylene to purify commercial styrene. The latter is a valuable monomer for manufacturing of polystyrene, unsaturated polyesters, styrene-butadiene rubbers and latexes, etc. [7].

Selective hydrogenation of acetylenic bonds is also of fundamental interest for fine organic synthesis. Importance of this reaction stems from that fact that substituted alkynes are versatile reagents in organic synthesis, because the –C≡CH group can be effectively used for formation of new carbon-carbon bonds with retention of the triple bond. Subsequent hydrogenation easily transforms di-substituted alkyne to a corresponding *cis*-alkene via a stereoselective addition of H_2 over Pd catalyst. This reaction is usually performed in the liquid-phase with high stereoselectivity to the target functionalized *cis*-alkenes, serving as a feedstock for pharmaceutical (e.g. synthesis of vitamins A, E, and K) and food industry, as well as production of liquid-crystal displays, detergents, etc. [8-11].

Generally, hydrogenation of acetylenic bond proceeds via two steps in accordance to the Horiuti-Polanyi mechanism [12]. At the first step alkyne is hydrogenated to an alkene, while

during the second step this alkene is further hydrogenated to the corresponding alkane. Two types of selectivity can be considered in such reactions. So-called thermodynamic selectivity is usually defined as the ratio between the adsorption energies of the alkyne and alkene [2, 13]. Thus, high thermodynamic selectivity implies that alkyne is preferably adsorbed on the catalyst surface inhibiting consecutive hydrogenation of the target alkene to the corresponding alkane. The second type is kinetic selectivity, which reflects the ratio of the rates in the first (semi-hydrogenation) and the second steps (over-hydrogenation) [2, 3, 14].

When performing selective hydrogenation it is important to control hydrogenation kinetically and to stop the process at the second step minimizing or preventing complete hydrogenation of the target olefin. From the kinetic viewpoint, it is desirable to maximize the ratio of the hydrogenation rates in the first (r_1) and the second steps (r_2). Thus, higher r_1/r_2 ratios permit easier control of the hydrogenation process either by interrupting the reaction after completion of the first step either by defining the reaction time in a batch reactor, or regulating the residence time in a fixed bed reactor. A typical catalyst for the liquid-phase alkyne hydrogenation is the so-called Lindlar catalyst based on Pd modified with Pb and supported on $CaCO_3$ [15, 16]. This catalyst provides a favorable r_1/r_2 ratio, suffering, however, from serious drawbacks such as the toxicity of lead and fast deactivation. In some cases, quinoline is also added to decelerate or even stop hydrogenation of the target *cis*-olefin due to stronger adsorption of quinoline thus enhancing selectivity [17]. However, a significant disadvantage of this method is the need for separation of quinoline from reaction products.

Several factors can be used to control selectivity and activity of Pd catalysts: formation of bi- and polymetallic alloy particles, variation of the support nature, or Pd particle size [14, 18-22]. Our previous studies have indicated that the size of Pd nanoparticles can significantly influence activity/selectivity parameters [18, 23] in substituted alkyne hydrogenation. It was found that an increase in the size of Pd nanoparticles increased TOF in acetylenic bond hydrogenation and the r_1/r_2 ratio thus favoring the kinetic control. However, to our knowledge,

the effect of Pd particle size on kinetics of selective hydrogenation of di-substituted internal alkynes is not studied in a sufficient detail, and no quantitative description of a relationship between the reaction rates in the first and the second hydrogenation steps and the metal particle size is available.

Two approaches have been proposed in the literature for quantification of the relationship between the metal particle size and the respective catalytic performance. The thermodynamic approach suggested in [24-26] considers changes in the chemical potential and thus the Gibbs energy as a function of the cluster size. To link thermodynamics with reaction kinetics and express dependence of the reaction rates and turnover frequency on the cluster size [27] the Brønsted-Evans-Polanyi relationship is applied making it possible to develop size-dependent rate equations for different mechanisms including the Eley-Rideal, the Langmuir-Hinshelwood mechanism and the two-step sequence. Such thermodynamic approach was applied for several catalytic reactions. Modelling was done in [24, 28, 29] for hydrogenation of crotonaldehyde over Au/TiO_2 [30] CO oxidation over gold [31], Fischer–Tropsch synthesis over Co-supported carbon nanofibers [32], allylic isomerization of allylbenzene to *trans*-β–methylstyrene over Au/Al_2O_3 [33], total oxidation of C_1-C_6 n-alkanes over nanosized Pt/Al_2O_3 [34, 35], oxidation of benzyl alcohol over silica - alumina supported palladium [36]. For each reaction, a good correspondence was obtained between the model predictions and experimental data indicating that thermodynamic approach could adequately depict dependence of structure sensitivity on the size of catalyst nanoparticles.

An alternative geometric approach considers directly crystallographic shapes of metal or metal oxide clusters. In this method, the rate constants are considered as size independent and each type of sites (different atoms in corners, edges and terraces) contributes to the overall reaction rate in accordance with their fraction in a cluster [37]. A mathematic model incorporating cluster size dependent rate constants was used to quantitatively describe

experimental data on TOF dependence on the metal particle size in catalytic hydrogenation of glucose, galactose and arabinose over Ru/C catalysts [38, 39]. The proposed model considers the average Ru particle size assuming a cubooctahedral shape of metal particles. Langmuir adsorption isotherm with noncompetitive adsorption of hydrogen was assumed for modeling. An adequate explanation of the experimental data was established [38, 39], showing that hydrogenation of sugars is a structure sensitive reaction with TOF maximum at ca. 3 nm.

The model similar to the one reported in [37] was also utilized in methane steam reforming to clarify the nature of the rate-controlling step [40].The intrinsic reaction rate was shown to decrease linearly with the metal dispersion suggesting that the overall reaction rate is controlled by the process occurring on the edge atoms of catalyst nanoparticles. The authors have concluded that the rate controlling step is CH_4 dissociation and CO formation occurring on the edge sites.

Both thermodynamic and geometric approaches were examined in [25] for ethene hydrogenation. Different reactivity of terraces and edges was found to be responsible for the cluster size effects. By comparison between experimental results and calculations using kinetic equations derived in [24, 28] the difference between the Gibbs energy of adsorption on edges and terraces could be computed. Additionally it was shown that TOF can change with the particle size due to changes in the coverage, while the rate constant is cluster size independent [25].

It can be concluded that while analysis of TOF as a function of the cluster size is available in the literature for some reactions, suitable kinetic models capable of describing kinetics of selective di-substituted alkynes hydrogenation in a batch reactor including concentration dependencies of the reaction products on the reaction time as a function of the Pd particle size are absent. The previous work of the authors reporting kinetic analysis of triple bond hydrogenation [41] was limited to phenylacetylene as a substrate and a formal thermodynamic approach. Therefore, the current research was focused on two main topics:

(1) Clarification of the effect of Pd particle size on activity and selectivity in the liquid-phase hydrogenation of disubstituted alkynes using diphenylacetylene (DPA) as a model substrate;

(2) Development of a kinetic model which can adequately describe the concentration dependencies over Pd supported catalyst upon variation of Pd particle size ranging from 1.9 to 20 nm. Selective hydrogenation of diphenylacetylene was chosen as a model reaction [9, 42, 43]. The detailed kinetic analysis was based on the geometrical model explicitly considering different reactivity of terraces, edges and corners, which according to our knowledge has never been applied before for description of time dependent concentration curves.

EXPERIMENTAL

Catalyst preparation

The parent γ-Al_2O_3 (Sasol TKA-432, S_{BET} = 215 m^2 g^{-1}, V_p = 1.25 cm^3 g^{-1}) support was crushed and sieved to the grain sizes between 0.25 and 0.50 mm and then calcined in dry air flow at 500°C for 2 h, treated with 20% acetic acid by incipient wetness followed by drying in air at room temperature overnight and then in an oven (120°C, 4 h). Thereafter, pretreated γ-Al_2O_3 was impregnated by the incipient wetness method with an aqueous $Pd(OAc)_2$ solutions acidified by concentrated HNO_3 and/or glacial acetic acid which were different in Pd-to-NO_3^- ratios. The impregnated materials were dried in a dry air flow (120°C, 3 h), calcined at 400 or 600°C (Table 1), and reduced in a 25% H_2/Ar flow (350°C, 3 h) followed by cooling in the flowing argon to ambient temperature. According to ICP-AES analysis, the metal content of 1 wt. % Pd was identical for all synthesized catalysts. More details on the catalyst preparation can be found elsewhere [44].

Because the size of Pd particles was varied by two parameters: (1) adjusting the acidification of $Pd(OAc)_2$ and (2) calcination temperature, the impregnating solution composition and the calcination temperature are summarized in Table 1 with the dispersion data

obtained by transmission electron microscopy and H_2 chemisorption. In all catalysts (Table 1) the number corresponds to the average Pd particle size.

Catalyst characterization

The specific area and porosity were obtained for the parent carrier and the prepared catalysts with an automatic "ASAP 2020 Plus" ("Micromeritics") Instrument using nitrogen as an adsorbate at the liquid nitrogen temperature (-196°C). Treatment in vacuum at 150 °C was applied prior to measurements. The specific surface area (S_{BET}) was calculated from the adsorption data in the relative pressure range between 0.05 and 0.20. The total pore volume (V_Σ) was evaluated at p/p_o =0.99.

Transmission electron microscopy (TEM) was utilized to define the average particle sizes for each synthesized sample and to analyze the Pd particle size distribution. The TEM images were collected with a JEM-2010 instrument (Jeol Co, Japan.) with an acceleration voltage of 200 kV and line-inline resolution of 0.14 nm. The powdered samples were ground and suspended in ethanol prior to measurements. Next, an ethanol suspension of the sample was deposited on a copper grid (d=3mm) followed by evaporation of ethanol. For a better contrast, the grid with sample was coated with a porous carbon. The size distribution was estimated by measuring 300–500 Pd particles for each sample. The average Pd particle size values determined by electron microscopy were used for revealing the particle size effect and structure sensitivity in the diphenylacetylene hydrogenation. Dispersion of Pd (D_{TEM}) was calculated on the basis of TEM data using an approximation suggested elsewhere [45].

Chemisorption was done using an Autosorb-1-C-MS/TCD analyzer (Quantachrome Instruments, USA). Pd dispersion ($D_{H2\ chem}$) was calculated from irreversible H_2 chemisorption data using a previously reported back sorption method [46]. Analysis was performed at 70°C in the pressure range of 1–100 mm Hg, assuming H/Pd stoichiometry equal to 1/1. After obtaining the first hydrogen isotherm, the samples were outgassed, and the second isotherm was obtained.

The hydrogen uptake was calculated from the irreversibly adsorbed H_2, as the difference between the first (total) and the second (reversible) isotherms in the pressure range 1-4 mm Hg.

The data on BET surface area, average size of Pd particles, and Pd dispersion for the catalysts under study are given in Table 1.

Catalytic tests

The liquid-phase hydrogenation of diphenylacetylene (DPA, 98%, Aldrich) was performed as described previously [20, 41]. A 10 ml vial used as a catalytic reactor was filled with the catalyst, DPA and *n*-hexane (98%, Merck) and then placed into the autoclave equipped with a gas supply line, liquid sampling units, and a magnetic stirrer. Typical catalytic tests were carried out at 25°C, initial hydrogen pressure of 5 bar, and 1000 rpm stirring.

Experiments with different catalyst amounts demonstrated that the gas-liquid mass transfer was not the limiting factor.

Special precautions were undertaken to ensure that the DPA hydrogenation was conducted in a kinetic regime avoiding external and internal mass-transfer limitations. External mass-transfer limitations were concluded to be avoided on the basis of the results of previous experiments with different stirring rates [47]. These data showed that at stirring rates exceeding 1000 rpm identical activity and selectivity were obtained. To minimize internal mass-transfer limitations the catalyst was fine grinded to obtain a powder with a particle size below 10 μm as suggested in [48].

Calculations of the Weisz-Prater criterion [49] for the highest reaction rate considering hydrogen concentration in the solvent and effective diffusion coefficient of hydrogen, a porosity to tortuosity ratio of 0.1, gave the values of the Weisz-Prater criterion below 0.02, ruling out internal mass transfer limitations.

The liquid samples were taken at regular intervals and analyzed by gas chromatography (GC) using a Crystal 5000 instrument (Chromatek, Russia) equipped with a flame-ionization detector and an HP5-MS column (5% phenyldimethylsiloxane; 30 m, 0.25 mm I.D., 0.25 μm

film thickness). A detailed analysis of the reaction products revealed that diphenylethylene (DPE) formation can be neglected up to DPA conversion of ca. 70% and that hydrogenation of the aromatic ring under the reaction conditions does not occur. This makes it possible to use H_2 consumption rate to evaluate DPA hydrogenation rates.

The amount of hydrogen uptake in the reaction was calculated from the pressure decrease during hydrogenation using an electronic pressure sensor connected with the autoclave. The pressure decrease was ca. 0.3 bar after complete hydrogenation, allowing neglecting the influence of H_2 pressure changes on the reaction kinetics.

The reaction rates r (mmol H_2 g_{Cat}^{-1} min^{-1}) were determined from the hydrogen uptake as a function of the reaction time [50] within uptake of 0.1 - 0.4 equivalent of H_2, and 1.1 - 1.3 equivalent of H_2 for DPA to DPE ($\boldsymbol{r}_1$) and DPE to diphenylethane (DPEt) rate ($\boldsymbol{r}_2$) hydrogenation, respectively. The obtained data were compared with the data determined via GC analysis of the reaction mixture after uptake of 0.1 to 0.4, and of 1.1 to1.3 equivalent of H_2 on the first and the second hydrogenation stage respectively. Both results were found to be in a good agreement (with deviation lower than +/- 2.5%).

Catalytic activity for each reaction step was evaluated from the values of turnover frequency (TOF, s^{-1}) and calculated as

$$TOF = r/60 * N_{Pd,surf.}^{-1}, \quad (1)$$

where r is the reaction rate (evaluated as mentioned above), and $N_{Pd,surf}$ is amount of surface Pd (mmol Pd_{surf}/gcat), calculated on the basis of dispersion D_{TEM} (Table 2), and taking into account that all catalysts contained 1 wt% Pd

$$N_{Pd,surf.} = 0.01*M_{Pd}^{-1}*D_{TEM}^{-1} \quad (2)$$

Efficiency of the kinetic control was evaluated by comparing the ratio of the hydrogenation rates (r_1/r_2) as it was previously proposed [17, 51].

Selectivity to the target product – diphenylethylene (S_{DPE}) was calculated using the following equation:

$$S_{DPE} = \frac{(C_{cis-DPE} + C_{trans-DPE})}{[(C_{cis-DPE} + C_{trans-DPE}) + C_{DPEt}]}, \quad (3)$$

where $C_{cis\text{-}DPE,}$ $C_{trans\text{-}DPE}$ and C_{DPEt} are concentrations of diphenylethylene (*cis*- and *trans*-) and diphenylethane (DPEt), respectively.

Stability tests

For these experiments Pd-4.8 and Pd-20 catalysts were recovered from the reaction mixtures by centrifugation (10 000 rpm, 10 min) after the end of DPA hydrogenation. The catalysts were then washed with *n*-hexane to ensure removal of the product from the catalyst surface and were dried overnight. Thereafter a new cycle of DPA hydrogenation was performed with the fresh solvent and reactants under the same conditions as the initial experiments.

RESULTS

Catalyst characterization

The average sizes of Pd nanoparticles calculated using TEM data according the equation suggested by Ichikawa et al. [45] are collected in Table 1. Fig. 1 shows the TEM micrographs, size distribution and EDS spectra of two synthesized catalysts with the smallest (Pd-1.9) and the largest (Pd-20) Pd particles.

Table 1. Preparation conditions, the average size of Pd particles (*d*), Pd dispersion determined by TEM (D_{TEM}) and H_2-chemisorption ($D_{H2\ chem.}$) and BET surface areas (S_{BET}) of the synthesized catalysts.

Sample	**Impregnating solution**	**Calcination conditions**	***d***	$\boldsymbol{D_{TEM}}^a$	$\boldsymbol{D_{H2\ chem.}}$	S_{BET}
			nm	**%**		**$m^2\ g^{-1}$**
Pd-1.9	$Pd(OAc)_2$ water solution acidified by concentrated HNO_3 (Pd^{2+}:NO_3^-=1:8)	400°C, 4 h	1.9	58.9	59.4	213
Pd-4.8		600°C, 2 h	4.8	23.3	26.7	208
Pd-5.7	$Pd(OAc)_2$ solution in 100% glacial acetic acid	600°C, 2 h	5.7	19.6	20.1	211
Pd-8.3	$Pd(OAc)_2$ solution in 50% acetic acid additionally acidified by concentrated HNO_3 (Pd^{2+}:NO_3^-=1:8)	400°C, 4 h	8.3	13.5	-	210
Pd-20		600°C, 2 h	20.0	5.6	5.9	214

[a] Calculated as D_{TEM}=1.12/*d*, in accordance with [45].

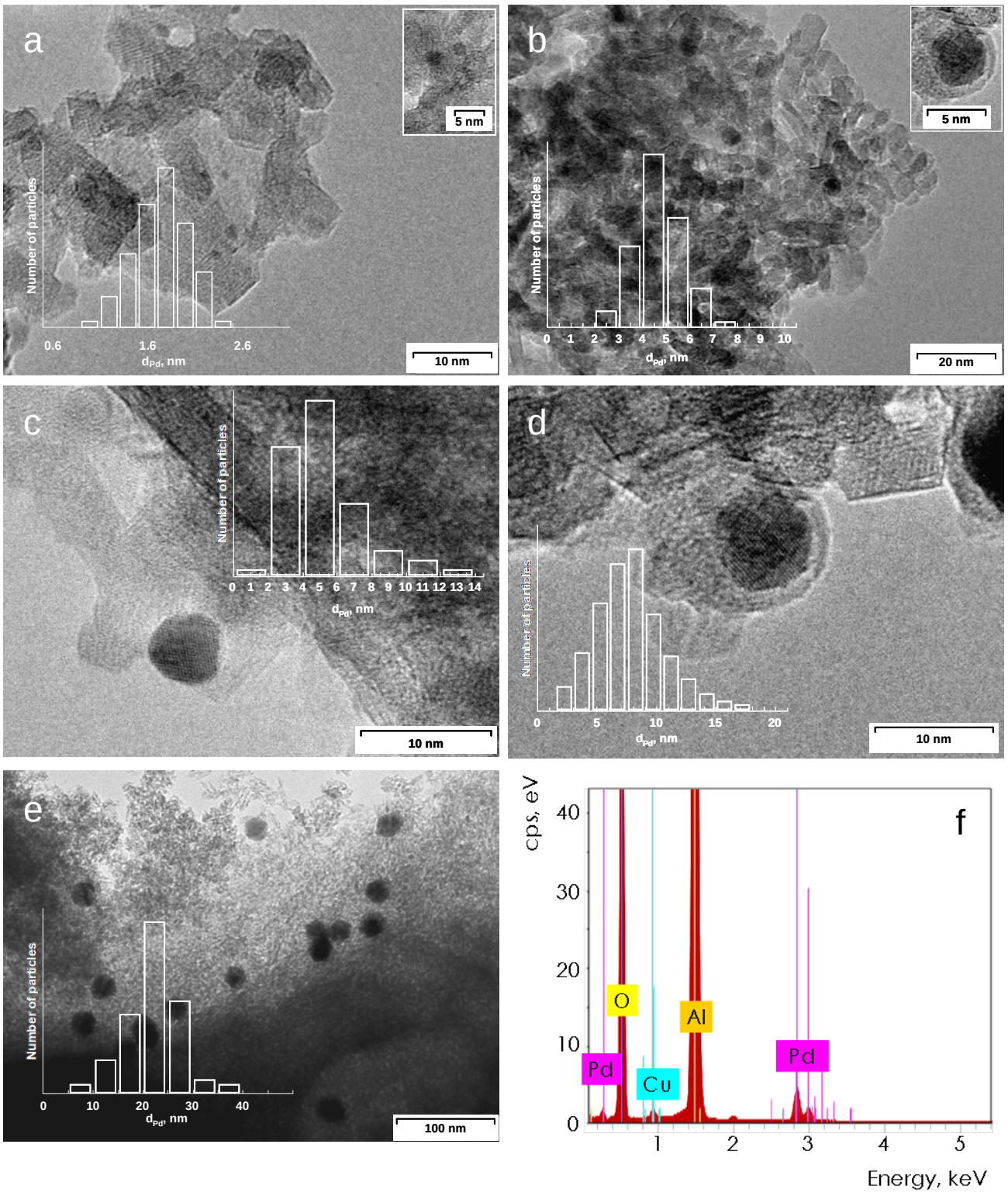

Fig. 1. TEM images and histograms of particle size distribution of 1%Pd/Al_2O_3 catalyst with the average particle sizes of 1.9 (a), 4.8 (b), 5.7 (c), 8.3 (d) and 20 nm (e). Part (f) represents characteristic EDS spectra.

The data indicate that both catalysts contain spherical or near-spherical nanoparticles with a cubo-octahedral shape typical for Pd fcc structure. The particle size distribution for finely

dispersed Pd catalyst is relatively narrow, around 1-2 nm, with a maximum at 1.9 nm (Fig. 1b). For the catalyst with the largest Pd particles size the distribution is broader being between 10 and 36 nm with the maximum at 20 nm (Fig. 1e). The average size in the latter case is also 20 nm.

Additionally, Pd dispersion for the catalysts with metal particles ranging from 1.9 to 4.8 nm was evaluated by H_2-chemisorption. The obtained values are in reasonable agreement with TEM data (Table 1).

Surface area measurements demonstrated that BET surface area of supported catalysts essentially did not change in the course of the catalyst preparation compared with the parent Al_2O_3 (Table 1). The values are almost identical for the parent γ-Al_2O_3 (215 m^2 g^{-1}) and the supported Pd/Al_2O_3 (ca. 208-214 m^2 g^{-1}). Presumably this stems from a low Pd loading and relatively wide alumina pores.

Catalytic data

Figure 2 shows typical kinetic profiles of hydrogen uptake in hydrogenation of diphenylacetylene over Pd/Al_2O_3 catalyst with Pd particle size varied from 1.9 to 20 nm.

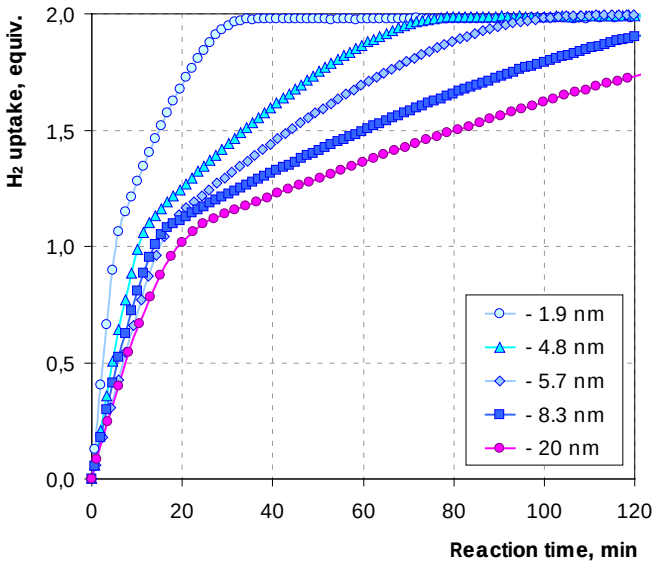

Fig. 2. Effect of Pd particle size on the kinetic performance of 1%Pd/Al_2O_3 catalyst in the liquid-phase hydrogenation of diphenylacetylene (DPA). Reaction conditions: $m_{1.9\ nm\text{-}8.3\ nm}$=1.5 mg; m_{20nm}=2.5 mg; P_{H2}= 5 bar; temperature 25 °C; [DPA]/Pd~4000; solvent: *n*-hexane.

The kinetic profiles of all catalysts exhibits a characteristic ~~downward bending~~ decrease of the slope after the uptake of one equivalent of H_2~~. Such bending~~ which clearly indicates a decrease in the hydrogenation rate after completion of the first step in DPA hydrogenation and beginning of the second step of the overall process (i.e. stilbene hydrogenation). The data obtained are consistent with previously reported results on DPA hydrogenation over Pd catalysts. Thus in [52, 53] the liquid-phase DPA hydrogenation was studied over Pd/MCM-41, Pd/zeolites and Pd/Al-PILC catalysts with 1 wt. % Pd loading and an average Pd particle size varied from 2-4 nm to 8-10 nm. The kinetic profiles for these catalysts display a similarly decreasing slope after an uptake of one equivalent of H_2 indicating a decrease in the hydrogenation rate at the stage of alkene hydrogenation.

Table 2 summarizes the hydrogenation rates for the first (r_1) and second (r_2) steps.

Table 2. Kinetics of the liquid-phase DPA hydrogenation over 1%Pd/Al_2O_3 .

Sample	r_1	r_2	r_1/r_2	TOF_1	TOF_2
	$\mu mol_{H2}\ g_{cat}^{-1}\ min^{-1}$			s^{-1}	
Pd-1.9	15.37	6.74	2.28	4.56	2.00
Pd-4.8	9.51	2.40	3.96	9.04	2.28
Pd-5.7	9.71	2.33	4.16	10.95	2.63
Pd-8.3	6.02	1.20	5.00	9.90	1.98
Pd-20	2.03	0.30	6.69	13.60	2.00
*TOF values were calculated based on D_{TEM} (see Experimental part for details).					

For the catalyst with the smallest particles (Pd-1.9) the rate of DPA hydrogenation (r_1~15.4 mmol H_2 g_{cat}^{-1} min^{-1}) is higher compared to stilbene hydrogenation (r_2 ~ 6.8 mmol H_2 g_{cat}^{-1} min^{-1}) resulting in the rate ratio r_1/r_2=2.3. It is noteworthy, that as the size of Pd particles increases the decreasing slope of the kinetic profile becomes more pronounced, indicating that stilbene hydrogenation becomes slower than hydrogenation of DPA. A systematic analysis of r_1/r_2 ratio for all investigated catalysts (Table 2) clearly shows a gradual increase in the r_1/r_2 ratio from ca. 2.3 to ca. 6.7 with an increase in the Pd particle size. As discussed in the Introduction,

such change in r_1/r_2 ratio facilitates the kinetic control and allows a possibility to efficiently interrupt the reaction after completion of the alkyne-to-olefin transformation preventing losses of the desired product [17, 50].

To reveal the effect of Pd particle size on diphenylacetylene hydrogenation kinetics it is informative to analyze the relationship between d_{Pd} and turnover frequencies of diphenylacetylene-to-stilbene (TOF_1) and stilbene-to-diphenylethane hydrogenation (TOF_2) (Fig. 3, Table 2).

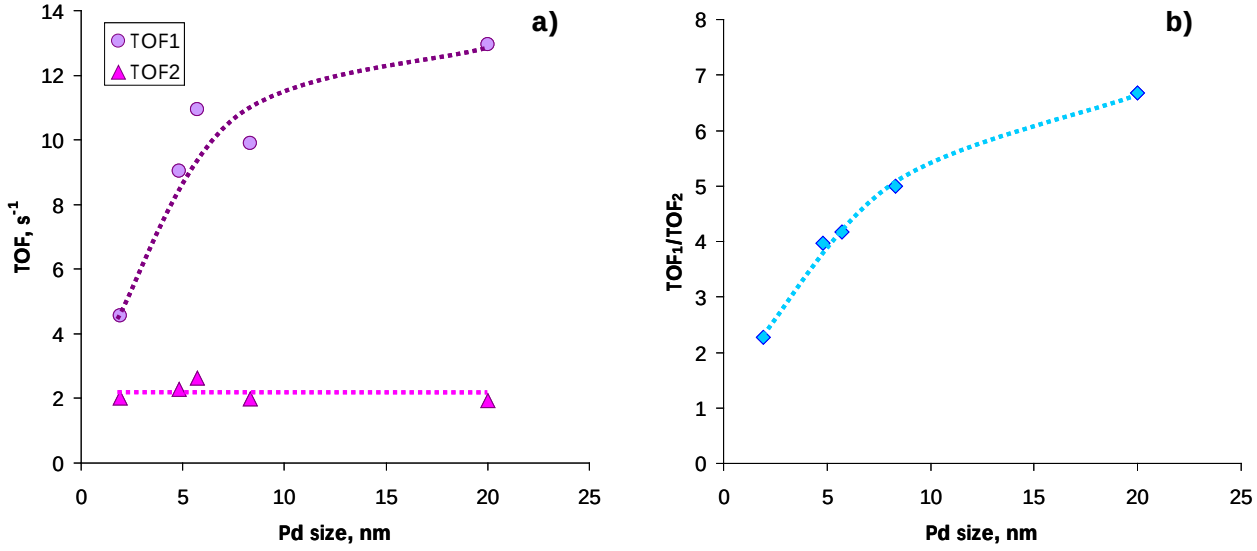

Fig. 3. Effect of Pd particle size on the turnover frequency of diphenylacetylene-to-stilbene (TOF_1) and stilbene-to-diphenylethane (TOF_2) hydrogenation. TOF values were calculated based on D_{TEM} (see Experimental part for details).

The obtained data show a significant increase in turnover frequency of the first reaction step for larger Pd particles. TOF_1 increases steadily from ~ 4.6 to ~ 13.6 s^{-1} as the diameter of Pd particles changes from 1.9 to 20 nm (Fig. 3a). This observation allows to conclude that hydrogenation of DPA to stilbene is a structure sensitive reaction. Remarkably, variation of the Pd particle size does not affect turnover frequency in the second reaction step (undesirable hydrogenation of stilbene intermediate to alkane): TOF_2 remains nearly constant ~ 2 s^{-1} within the whole range of Pd particle sizes studied in the current work.

Such variations of TOF_1, TOF_2, and r_1/r_2 ratio with Pd particle size should inevitably affect selectivity in stilbene formation. It is thus meaningful to analyze time dependencies of the reaction product concentrations and selectivity for catalysts with different Pd particle sizes.

Variations of the reaction product concentrations as a function of the reaction time for the catalyst with the smallest (Pd-1.9) and the largest Pd particles (Pd-20) are compared in Fig. 4.

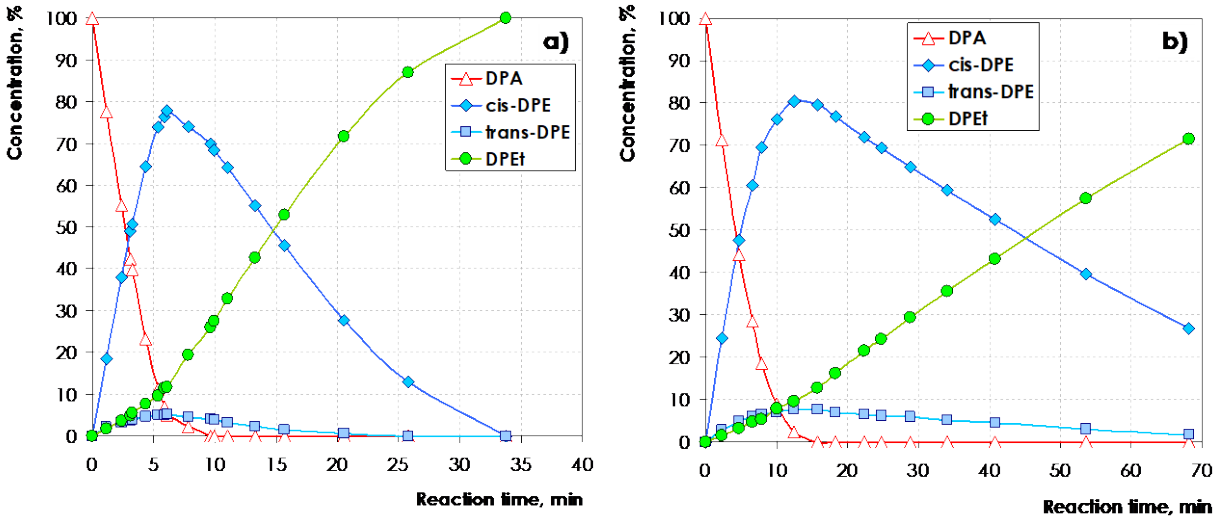

Fig. 4. Products distribution for Pd/Al_2O_3 catalysts with Pd sizes of 1.9 (a) and 20 nm (b). DPA – Diphenylacetylene, *cis*-/*trans*-DPE – *cis*-/*trans*-Diphenylacetylene, DPEt – Diphenylethane.

The concentration profile of stilbene is consistent with the consecutive reaction mechanism, suggesting that DPA hydrogenation leads to formation of the alkene following by its transformation to the alkane in the second step. For both catalysts diphenylethane appears as the reaction product even at low DPA conversion.

Visualization of the relationship between selectivity to alkene as a function of DPA conversion and the Pd particle size is displayed in Fig. 5. This figure illustrates that selectivity to stilbene is not 100% even at low conversion, being rather constant up to conversion levels of ca. 50% for all catalysts apart from the one with the lowest cluster size. From the mechanistic viewpoint these observations imply that direct hydrogenation of the triple bond to the alkane should be introduced in the reaction mechanism. When DPA hydrogenation is complete, differences between Pd-20 and Pd-1.9 became apparent. Thus, for Pd-20 the concentration of diphenylethane remained below 12%, while for Pd-1.9 this value is almost 30%. These data

indicate that for larger Pd particles sizes a contribution of the total hydrogenation to the overall process tends to decrease. This leads to an increase in the yield of the desired alkene intermediate improving selectivity [54].

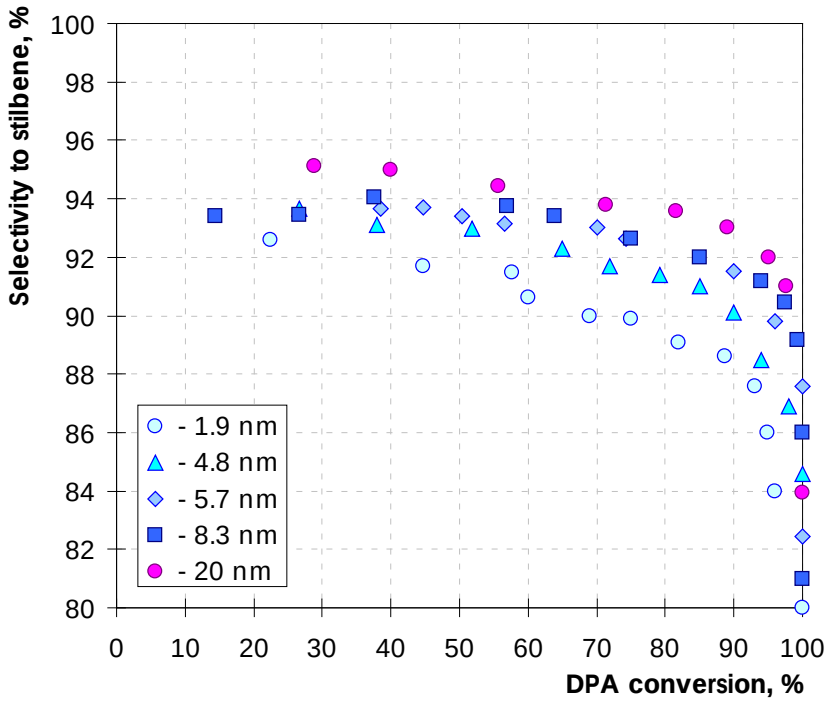

Fig. 5. Selectivity to alkene as a function of DPA conversion over Pd/Al_2O_3 catalysts with different Pd sizes. Reaction conditions: $m_{1.9\ nm\text{-}8.3\ nm}$=1.5 mg; m_{20nm}=2.5 mg; P_{H2}= 5 bar; temperature 25 °C; [DPA]/Pd~4000; solvent: *n*-hexane.

At low DPA conversion, selectivity is below 100% for all catalysts meaning that even at the beginning of the reaction diphenylethane is detected as the reaction product, which is also apparently clear from the time-dependent concentration profiles (Fig. 4). Figure 5 illustrates that selectivity to stilbene can be elevated with an increase in the size of Pd nanoparticles.

For instance, at the DPA conversion of ca. 80%, selectivity toward stilbene is ca. 84-88% and ca. 91-94% for Pd-1.9 and Pd-20 catalysts, respectively. In fact, Pd-1.9 catalyst exhibited selectivity lower in comparison to other catalysts within the whole range of DPA conversion. As

Pd particles increases in size, selectivity is gradually improved and the “selectivity vs DPA conversion” profiles are becoming closer to the profile of the most selective Pd-20 catalyst.

The obtained data allow suggesting that the observed relationship between the catalytic performance and the size of Pd nanoparticles stems from different structure sensitivity behavior in alkyne and alkene hydrogenation. Therefore, it is informative to analyze and compare the results of the current work on structure sensitivity in hydrogenation of DPA and stilbene with the available literature data for similar molecules (Table S1).

In our previous study the particle size effect was investigated in the liquid-phase hydrogenation of phenylacetylene [41]. Hydrogenation of the triple bond was found to be structure sensitive and turnover frequency on the first hydrogenation stage (TOF_1) increased by 14 times with the increase in Pd particle size from 1.5 and 22.0 nm. For the second stage of styrene hydrogenation structure sensitivity was significantly less pronounced and the turnover frequency (TOF_2) increased only by 3.8 times. Due to the different structure sensitivities at the first and the second hydrogenation stages TOF_1/TOF_2 tends to increase fourfold from 0.4 to 1.6. These data are in qualitative agreement with different structure sensitivity for alkyne and alkene hydrogenation observed in this study resulting in a threefold TOF_1/TOF_2 increase from 2.3 to 6.7 (see Fig. 3b).

In should be mentioned that in phenylacetylene hydrogenation structure sensitivity is more pronounced compared to DPA hydrogenation. Thus TOF_2 in phenylacetylene hydrogenation increases from 5.7 to 21.9 s^{-1}, while in DPA hydrogenation TOF_2 was found to be essentially independent on the Pd particle size (see Fig. 3a). Tentatively this difference can be attributed to different geometry and reactivity of phenylacetylene and diphenylacetylene leading to different adsorption geometry and adsorption site requirement. Clearly an additional study using comparative DFT modeling of adsorption and activation of phenylacetylene and diphenylacetylene molecules on Pd surface is required to clarify the observed differences in structure sensitivity.

Pronounced structure sensitivity in alkyne hydrogenation was also reported by other authors. Thus, in phenylacetylene hydrogenation Domingues-Domingues et al. observed a seven fold TOF_1 increase as the size of Pd particles increased from 2 to 13 nm [55]. An analogous trend in phenylacetylene hydrogenation was reported by Quek et al. [56]. The particle size effect was shown to have a strong influence on the activity in acetylene hydrogenation [57]. In the latter study it was found that TOF dropped by 85% when the Pd particle size decreased from 3.6 to 2.1 nm. All these observations indicate that the turnover frequency of acetylenic bond hydrogenation to double bond tends to increase with increasing Pd particle size.

A possible interpretation for the observed structure sensitivity in alkyne hydrogenation on Pd was proposed by Semagina et al. [58]. The authors revealed a 15-fold TOF increase in 1-hexyne hydrogenation as Pd particle diameter increased from 11 to 14 nm. The experimental results were explained by a “geometric” nature of the size effect, suggesting that an ensemble of several neighboring Pd surface atoms is necessary to constitute the active center responsible for hydrogenation. Thus, the largest ensemble of surface atoms is required for π-adsorbed or di-σ-adsorbed flat-lying alkynes, which may occupy up to five surface Pd atoms. As Pd particles increase in size, their larger facets provide more planar space for a flat-lying alkyne being, therefore, more catalytically active [14]. It should be taken into account that after completion of the first hydrogenation step, flat-lying alkyne is transformed to less symmetrical bended Z-alkene molecule requiring a smaller space on the surface for adsorption, thereby diminishing the size effect on turnover frequency as will be elaborated further. These experimental results show that calculations of the turnover frequency per exposed surface atom might not be completely relevant when a large organic molecule is reacting and a multi-atomic surface site is required to accommodate the reacting molecules.

Similar arguments were recently presented in line with the ensemble theory in catalysis requiring availability of specific ensembles of surface atoms [59]. The concept of ensembles is also consistent with the notion of multisite adsorption, which is often applied to describe kinetics

of complex organic reactions. For example, importance of multisite adsorption and its influence on the reaction kinetics has been demonstrated by Bernas at al. [60]. It was found that in hydrogenolysis of a lignan-hydroxymatairesinol (HMR) reaction kinetics can be adequately describe only assuming occupation of several surface sites on Pd/C catalyst upon HMR adsorption.

In addition to geometric requirements of multisite adsorption, some recent DFT calculations of the adsorption energy of alkyne molecule on edges, corners, and plane sites of Pd nanoparticles revealed importance of the facets for the molecule activation. Preference of the plane sites was clearly demonstrated by a DFT investigation of 2-methyl-3-butyn-2-ol (MBY) and 2-methyl-3-buten-2-ol (MBE) adsorption and hydrogenation on a Pd30 cluster, exhibiting both {100} and {111} faces and low coordination sites [61]. It was demonstrated that the alkyne adsorption by the C-C bond on the plane sites results in the molecule interactions by two types of bridge coordination with four and three Pd atoms. These configurations are characterized by an elongation of C-C bond of ca. 17% and 13% significant interaction energies of ca. 175-210 kJ/mol. On the other hand, adsorption of alkyne molecule on corner and edge sites results in surface species interacting with just one or two Pd atoms and the corresponding C-C bond elongation only by 5 or 9% respectively (interaction energies ~ 90-135 kJ/mol). DFT-investigations of hydrogenation indicated that the involved energy barriers are very similar for different intermediates, allowing to conclude that structure sensitivity is governed by adsorption (the thermodynamic factor), rather than the height of hydrogenation barriers. The results of DFT calculations were found to be in an excellent agreement with the experimental results [62].

It is remarkable that a DFT study of MBE hydrogenation showed that hydrogenation of an alkene exhibits significantly less pronounced structure sensitivity than that for alkynes. According to the calculations, the differences in C=C bond elongation in the case of olefin adsorption on plane, edge, and corner sites were found to be relatively small (ca. 4%) as compared to the C-C bond elongation in an adsorbed alkyne (13 - 17%). Adsorption energies are

also on average lower for MBE with respect to surface species derived from MBY. It is noteworthy that the observed differences in structure sensitivity are in line with available literature data indicating that in alkenes hydrogenation, in contrast to alkynes, specific catalytic activity does not depend strongly on the Pd particle size. In most cases for alkene hydrogenation turnover frequency changes less than two- or threefold as the particle size changes within a range of 1–10nm implying lower structure sensitivity of olefin hydrogenation [63, 64].

Thus, the available experimental and theoretical data reveal high structure sensitivity of alkyne hydrogenation and indicate that the predominance of the plane sites on Pd nanoparticle surface favors hydrogenation of alkyne molecules from both geometric and energetic viewpoints. Therefore, the observed increase in TOF_1 for larger Pd particles can be attributed to the increased fraction of plane sites (Table S1). On the other hand, lower structure sensitivity in alkene hydrogenation leads to essentially independence of TOF_2 on Pd particle diameter within 2 - 20 nm size range.

Catalyst stability

To evaluate possible impact of the reaction conditions on Pd particle size, Pd-4.8 and Pd-20 catalysts were investigated in the repeated catalytic tests. The data are collected in Table S2 and Figs. S1 and S2. These result confirmed that the catalytic performance of the fresh and recycled samples is essentially identical, which suggest the absence of noticeable changes in Pd dispersion in the course of catalytic reaction.

Reaction network

Prior to development of a kinetic model incorporating the cluster size effect the reaction network accounting for concentration dependencies in diphenylacetylene hydrogenation should be considered. Such reaction mechanism takes the following form:

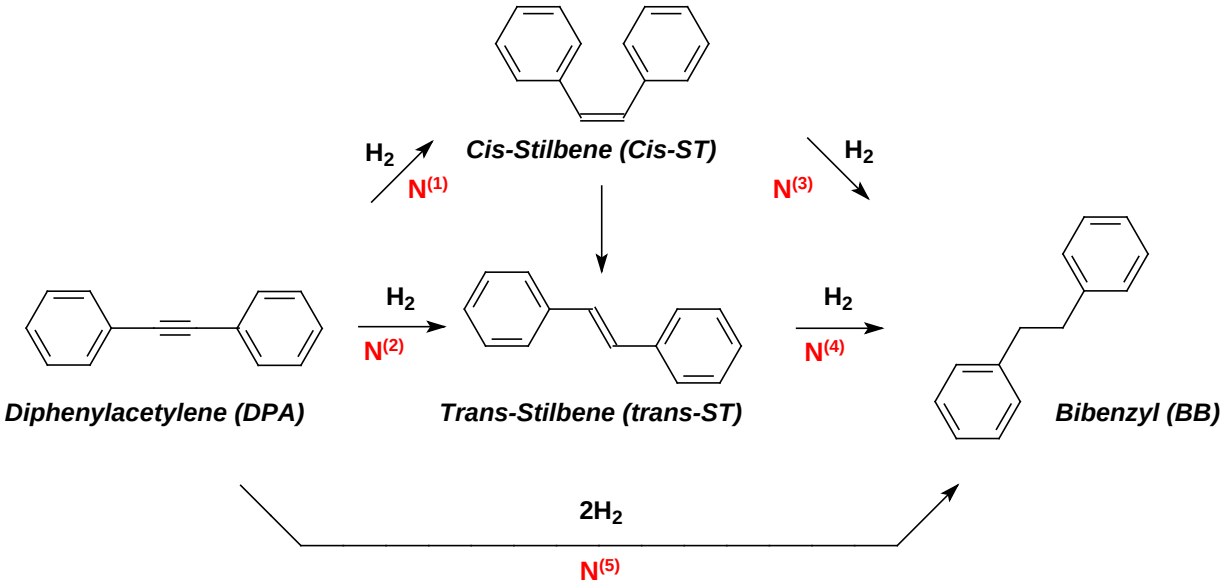

	$N^{(1)}$	$N^{(2)}$	$N^{(3)}$	$N^{(4)}$	$N^{(5)}$	
1. A* +H_2→C*	1	0	0	0	0	
2. A*+H_2→T*	0	1	0	0	0	
3. C* +H_2→P*	0	0	1	0	0	
4. T*+H_2→P*	0	0	0	1	0	
5. A* +2H_2→P*	0	0	0	0	1	(4)
6.A+*=A*	1	1	0	0	1	
7. C+*=C*	-1	0	1	0	0	
8. T+*=T*	0	-1	0	1	0	
9. P+*=P*	0	0	-1	-1	-1	

$N^{(1)}$ A+H_2→C; $N^{(2)}$ A+H_2→T; $N^{(3)}$ C+H_2→P; $N^{(4)}$ T+H_2→P; $N^{(5)}$ A+2H_2→P

On the right hand side of the equations for the steps the stoichiometric (or Horiuti) numbers along the routes $N^{(1)}$ - $N^{(3)}$ are given [65]. Steps 6-9 are considered at quasi-equilibria. In eq. (4) A stands for DPA, C and T represent respectively *cis*- and *trans*-stilbene, while P corresponds to diphenylethane and * denotes a surface site. Representation of the reaction mechanism in terms of hydrogen involvement is somewhat simplified because all experiments in

the current work were done at the same hydrogen pressure. Apparently, elementary steps can be more complex including for example adsorption and dissociation of hydrogen.

As discussed above the route $N^{(5)}$ is included in the reaction mechanism to account for direct hydrogenation of the triple bond to the alkane similar to hydrogenation of acetylene to ethane [66-68]. Step 5 in eq. (4) does not necessarily mean that two hydrogen molecules are added simultaneously and is more complicated. Discrimination between different mechanisms for the route $N^{(5)}$ cannot be done using the current set of experimental data generated at the same hydrogen pressure. Moreover, introduction of 13C labeled stilbene might be required to confirm the direct hydrogenation route from DPA to the corresponding alkane.

The rate expressions for the reaction routes can be written as follows:

$$r^{(I)} = \frac{k_1 K_6 N_A}{1 + K_6 N_A + K_7 N_C + K_8 N_T + K_9 N_P} \quad (5)$$

$$r^{(II)} = \frac{k_2 K_6 N_A}{1 + K_6 N_A + K_7 N_C + K_8 N_T + K_9 N_P} \quad (6)$$

$$r^{(III)} = \frac{k_3 K_7 N_C}{1 + K_6 N_A + K_7 N_C + K_8 N_T + K_9 N_P} \quad (7)$$

$$r^{(IV)} = \frac{k_4 K_8 N_T}{1 + K_6 N_A + K_7 N_C + K_8 N_T + K_9 N_P} \quad (8)$$

$$r^{(V)} = \frac{k_5 K_6 N_A}{1 + K_6 N_A + K_7 N_C + K_8 N_T + K_9 N_P} \quad (9)$$

Here k_1, etc. are the rate constants, including hydrogen pressure dependence, K_6 are equilibrium constants for respective steps, etc., N_A is the mole fraction of reactant A, etc; $r^{(I)}$, etc., stand for reaction rates along the respective routes in eq. (1).

Eq. (5-9) should be solved together with the mass balances for different components in a batch reactor

$$-\frac{n}{mD}\frac{dN_A}{dt} = r^{(I)} + r^{(II)} + r^{(V)};\ \frac{n}{mD}\frac{dN_C}{dt} = r^{(I)} - r^{(III)};$$

$$\frac{n}{mD}\frac{dN_T}{dt} = r^{(II)} - r^{(IV)};\frac{n}{mD}\frac{dN_P}{dt} = r^{(III)} + r^{(IV)} + r^{(V)} \quad (10)$$

where *m* is the mass of catalyst, *n* is the initial amount of DPA in moles loaded in the reactor and D is the metal dispersion.

Size dependent kinetics

In line with the discussion above, analysis of the cluster size dependent kinetics to treat structure sensitivity was based on recognition of distinct active sites. The rate constants were considered as size independent, while the reaction was assumed to occur on several types of active sites. Such sites are chemically different being palladium atoms (ensembles) present either in edges, corners or terraces. Then each type of sites contributes to the overall rate according to their relative fractions f by the following expression:

$$r = r_{terraces} f_{terraces} + r_{edges} f_{edges} + r_{corners} f_{corners} \quad (11)$$

Theoretical analysis for the two- step reaction mechanism was presented in [69].

Different geometrical models can be in general used to represent the metal clusters [70], such as a simple cubic or a more complex cuboctahedron model was used. For the sake of simplicity, it can be considered for both models that activity of atoms in corners and edges is the same. The fraction of terraces can be calculated as for the cubic (eq. 12) and a cubo-octahedron (eq. 13) models:

$$f_{terraces,cubic} = \frac{n_{atoms\_terraces}}{n_{all\_surface\_atoms}} = \frac{6(m-1)^2 + 6(m-2)^2}{12m^2 - 24m + 14} \quad (12)$$

$$f_{terraces,cubooctahedra} = \frac{n_{atoms\_terraces}}{n_{all\_surface\_atoms}} = \frac{8(3m^2 - 9m + 7)^2 + 6(m-2)^2}{30m^2 - 60m + 32} \quad (13)$$

where *m* is related to the cluster size and the atom diameter

$$m = \frac{d_{cluster}}{2d_{at}} \tag{14}$$

In the current work the cubo-octahedron representation (eq. 13) was adopted. In this context it was interesting to analyse data in Fig. 3 using eq. (11) with the fraction of terraces given by eq. (13). It is clear from Fig. S3, that the model is able in general to capture the cluster size dependence even if at largest cluster size the experimentally observed value of TOF is larger than theoretically predicted using a kinetic free model for cubo-octahedron, i.e. eq. 11.

For modelling of the concentration curves the expressions for the reaction rates per exposed sites along different routes (eqs. 15-19) were solved together with the mass balances (eq. 10).

$$r^{(I)} = \frac{k_{1,e}K_{6,e}N_A}{1+K_{6,e}N_A+K_{7,e}N_C+K_{8,e}N_T+K_{9,e}N_P}(1-f_{terraces})+ \\ +\frac{k_{1,t}K_{6,t}N_A}{1+K_{6,t}N_A+K_{7,t}N_C+K_{8,t}N_T+K_{9,t}N_P}f_{terraces} \tag{15}$$

$$r^{(II)} = \frac{k_{2,e}K_{6,e}N_A}{1+K_{6,e}N_A+K_{7,e}N_C+K_{8,e}N_T+K_{9,e}N_P}(1-f_{terraces})+ \\ +\frac{k_{2,t}K_{6,t}N_A}{1+K_{6,t}N_A+K_{7,t}N_C+K_{8,t}N_T+K_{9,t}N_P}f_{terraces} \tag{16}$$

$$r^{(III)} = \frac{k_{3,e}K_{7,e}N_A}{1+K_{6,e}N_A+K_{7,e}N_C+K_{8,e}N_T+K_{9,e}N_P}(1-f_{terraces})+ \\ +\frac{k_{3,t}K_{7,t}N_A}{1+K_{6,t}N_A+K_{7,t}N_C+K_{8,t}N_T+K_{9,t}N_P}f_{terraces} \tag{17}$$

$$r^{(IV)} = \frac{k_{4,e}K_{8,e}N_A}{1+K_{6,e}N_A+K_{7,e}N_C+K_{8,e}N_T+K_{9,e}N_P}(1-f_{terraces})+ \\ +\frac{k_{4,t}K_{8,t}N_A}{1+K_{6,t}N_A+K_{7,t}N_C+K_{8,t}N_T+K_{9,t}N_P}f_{terraces} \tag{18}$$

$$r^{(V)} = \frac{k_{5,e}K_{6,e}N_A}{1+K_{6,e}N_A+K_{7,e}N_C+K_{8,e}N_T+K_{9,e}N_P}(1-f_{terraces})+ \\ +\frac{k_{5,t}K_{6,t}N_A}{1+K_{6,t}N_A+K_{7,t}N_C+K_{8,t}N_T+K_{9,t}N_P}f_{terraces} \tag{19}$$

Kinetic modeling was performed using ModEst software [71]. The objective function (Q) for the residual sum of squares between the calculated and experimental data was minimized during the parameter estimation to search for the best-fit values using the Levenberg−Marquardt algorithm implemented in the software. The error function is defined as:

$$Q = \sum\left(C_{i,t\,(est)} - C_{i,t\,(\exp)}\right)^2 \qquad (20)$$

where *i* and *t* denote the components and the corresponding times, respectively.

The accuracy of the model description was determined with the R^2 – coefficient or degree of explanation, which reflects comparison between the residuals given by the model with the residuals of the simplest model, i.e. the average value of all data points [72]. The R^2 value is given by expression:

$$R^2 = 100\frac{\left(y_{model} - y_{experiment}\right)^2}{\left(y_{model} - \bar{y}_{experiment}\right)^2} \qquad (21)$$

Because TOF is hydrogenation of stilbene is independent of the cluster size in the calculations the values of rate constants for step 3 on edges and terraces along with respective adsorption constants were considered to be equal to each other $k_{3,e} = k_{3,t} = k_3$, $K_{7,e} = K_{7,t} = K_7$. The same approach was adapted for the step 4 $k_{4,e} = k_{4,t} = k_4$ and $K_{8,e} = K_{8,t} = K_8$. For the sake of simplicity and considering a minor contribution of the route $N(^V)$ to generation of the final product only contribution of terraces was supposed.

Application of eq. (15-19) along with the mass balance equation (10) gave a reliable description of experimental data (Fig. 6) with the degree of explanation equal 97.7%. The values of parameters are presented in Table 3.

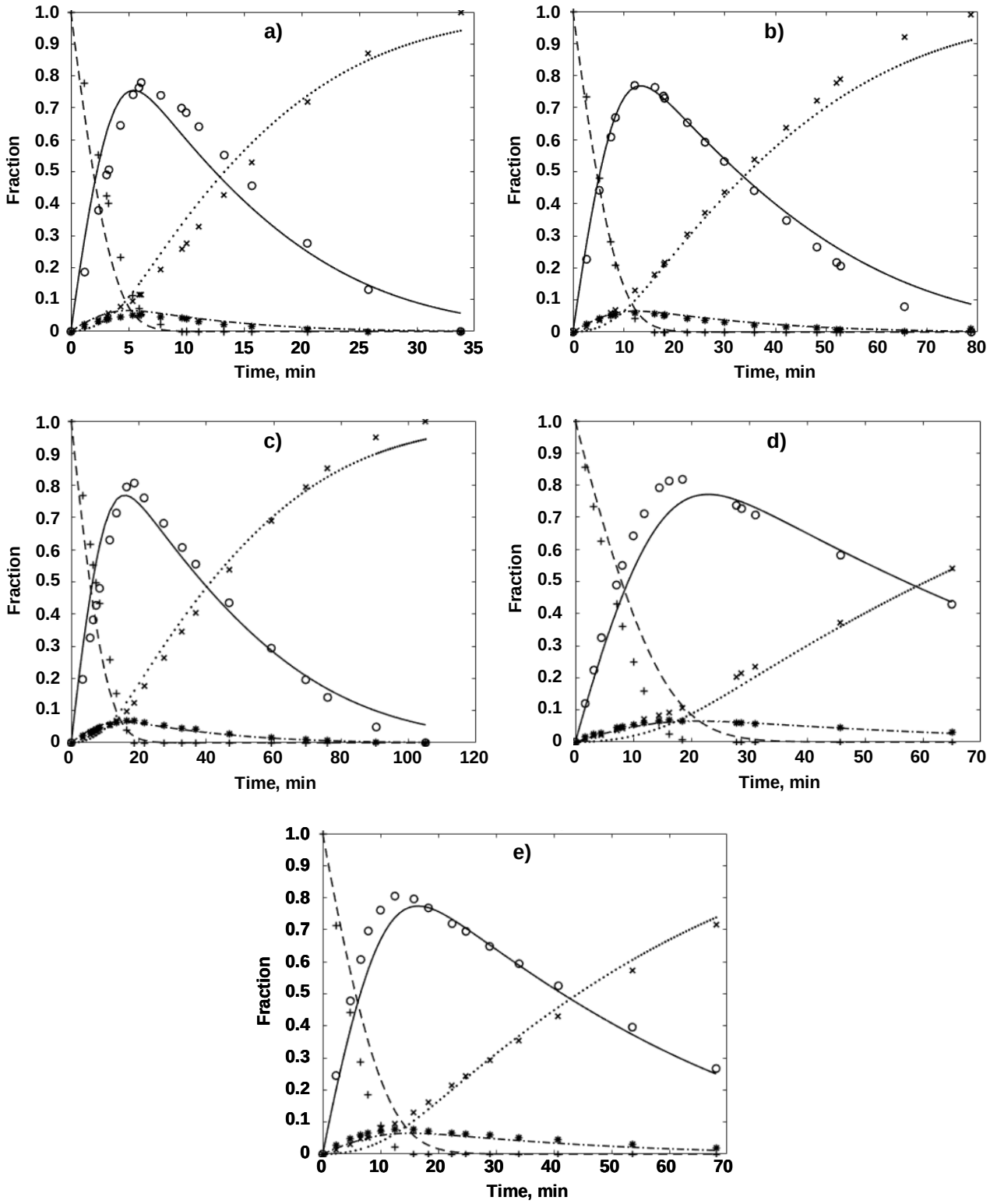

Fig. 6. Comparison between experimental (symbols) and calculated data (lines) in hydrogenation of diphenylacetylene over Pd catalysts with different dispersion: a) 1.9 nm, b) 4.8 nm, c) 5.7 nm, d) 8.3 nm, e) 20 nm.

Table 3. Values of kinetic parameters for the model represented by eq. (15-19).

Parameter	Value	Error, %	Units
$k_{1,t}K_{6,t}m/n$	3.5	22.6	min^{-1}
$k_{2,t}K_{6,t}m/n$	0.30	36.9	min^{-1}
$k_{1,e}K_{6,e}m/n$	0.039	>100	min^{-1}
$k_{2,e}K_{6,e}m/n$	0.069	>100	min^{-1}
k_3K_7m/n	0.21	15.7	min^{-1}
k_4K_8m/n	0.28	45.2	min^{-1}
$k_{5,t}K_{6,t}m/n$	0.016	>100	min^{-1}
$K_{6,t}$	8.8	26.4	-
$K_{6,e}$	8.1	>100	-
$K_{7,t}$	2.2	32	-

In general, the parameters are rather well-identified and that only few parameters are correlating with each other. The relative ratio between $k_{1,t}K_{6,t}m/n$ and $k_{2,t}K_{6,t}m/n$ is in line with high selectivity to *cis*-stilbene. As expected, the contribution of reactions on edges is much smaller than on terraces, therefore there were large errors in the values of the rate constants $k_{1,e}K_{6,e}m/n$ and $k_{2,e}K_{6,e}m/n$. The adsorption coefficient of DPA on edges was according to calculations of the same magnitude as for terraces, however, the error was too high to allow meaning discussion on its physical meaning.

Values of $k_{1,t}K_{6,t}m/n$ and k_3K_7m/n rather than just values of adsorption parameters K_6 and K_7 determine the ratio of r_1 to r_2 being in line with experimentally observed selectivity to stilbene.

The correlation matrix of the parameters is given in Supporting Information (Table S3), while the statistical data obtained from Markov Chain Monte Carlo (MCMC) method are presented in Figs. S4 and S5. These figures display the most probable values of constants as

maxima. The MCMC method, incorporated in the optimization software ModEst, provides a tool for the evaluation of the reliability of the model parameters by treating all the uncertainties in the data and the modelling as statistical distributions [73]. The parameter estimation results are usually described by contour plots relating two parameters, which might in general have a mutual compensation. While elongated contour plots point out a strong correlation between parameters, the contours consisting of circles, as displayed in Fig. S4 point out on a negligible correlation between parameters.

CONCLUSIONS

This study was devoted to the detailed study of particle size effect in liquid phase hydrogenation of substituted alkynes. The main focus of the research was the development of the relevant kinetic models capable to capture a relationship between Pd particle size and kinetics of liquid phase selective hydrogenation of substituted alkynes in a batch reactor including concentration dependencies of the reaction products on the reaction time. The study was carried out using representative series of Pd/Al_2O_3 catalysts with identical Pd loading (~ 1.0 wt%) and different size of Pd particles ranging from 1.9 to 20.0 nm. Hydrogenation was carried out at ambient temperature and H_2 pressure of 5 bars using diphenylacetylene as a model molecule.

The data obtained revealed significantly different relationships between Pd particle sizes and turnover frequency for alkyne and an intermediate alkene hydrogenation (TOF_1 and TOF_2 respectively). TOF_1 gradually increased from ~ 4.6 to ~ 13.6 s^{-1} as the diameter of Pd particles was changing from 1.9 to 20 nm. On the other hand, for all catalysts under study TOF_2 remains essentially constant (~2 s^{-1}) and independent on the size of Pd nanoparticles. There observation suggests different structure sensitivity behavior in alkyne and alkene hydrogenation.

Different structure sensitivity in the first and second hydrogenation steps results in markedly different reaction kinetics for the catalysts with either small or large Pd nanoparticles. It was found that because the TOF_1/TOF_2 ratio increases in parallel with the size of Pd, hydrogenation rate significantly slows down after completion of the alkyne hydrogenation stage, and the profile of hydrogen uptake exhibits a pronounced decrease of the slope after consumption of one H_2 eqvivalent for catalysts bearing larger Pd particles. Such changes in the reaction kinetics facilitate kinetic control of the reaction by interrupting hydrogenation to minimize undesirable overhydrogenation. An increase in the TOF_1/TOF_2 ratio also favors selectivity in alkene formation for the catalysts with larger Pd particles.

The effect of Pd nanoparticle size on the hydrogenation kinetics was analyzed and quantitatively interpreted using the geometric approach, which explicitly considers crystallographic shapes of

the active metal and contributions of different active sites in accordance with their reactivity. The kinetic model was developed with size independent rate constants, which contribute to the overall reaction according to the fraction of chemically different palladium ensembles present either in edges, corners or terraces.

In the case of structure insensitive stilbene hydrogenation the values of rate constants on edges and terraces along with respective adsorption constants equal to each other, while for hydrogenation of diphenylacetylene the contribution of reactions on edges is much smaller than on terraces.

The advanced model was able to describe in a reliable way concentration profiles of all components at different cluster sized of palladium.

Acknowledgement

Authors are grateful to Dr. Evgeny Gerasimov from Boreskov Institute of Catalysis SB RAS for studying the samples by TEM.

REFERENCES

1. H.-U. Blaser, A. Schnyder, H. Steiner, F. Rössler and P. Baumeister, in Handbook of Heterogeneous Catalysis, Wiley-VCH, Weinheim, 2008, pp. 3284–3308.
2. A. Borodzinski, G. C. Bond, Catal. Rev. -Sci. Eng. 48 (2006) 91-144.
3. A. Borodzinski, G. C. Bond, Catal. Rev. -Sci. Eng. 50 (2008) 379-469.
4. J. Osswald, Active-Site Isolation for the Selective Hydrogenation of Acetylene: the Pd-Ga and Pd-Sn Intermetallic Compounds, Doctoral Thesis, Technische Universität Berlin, Fakultät II - Mathematik und Naturwissenschaften, 2005, p. 10.
5. M. Takht Ravanchi, S. Sahebdelfar, S. Komeili, Rev. Chem. Eng. 34(2) (2018) 215–237.
6. R. Hou (2017) Introduction. In: Catalytic and Process Study of the Selective Hydrogenation of Acetylene and 1,3-Butadiene. Springer Theses (Recognizing Outstanding Ph.D. Research). Springer, Singapore.
7. A. V. Rassolov, P. V. Markov, G. O. Bragina, G. N. Baeva, I. S. Mashkovskii, I. A. Yakushev, M. N. Vargaftik, A. Yu. Stakheev, Kinet. Catal. 57 (2016) 853–858.
8. W. Bonrath, J. Medlock, J. Schütz, B. Wüstenberg, T. Netscher, Hydrogenation in the Vitamins and Fine Chemicals Industry—An Overview, Hydrogenation, Karamé, I., Ed., InTech, Rijeka, 2012, pp. 69-90.
9. S. Furukawa, A. Yokoyama, T. Komatsu, ACS Catal. 4 (2014) 3581-3585.
10. K. Ichimura, Chem. Rev. 100 (2000) 1847-1874.
11. M. Halim, I.D.W. Samuel, J.N.G. Pillow, A.P. Monkman, P.L. Burn, Synth. Met. 102 (1999) 1571-1574.
12. M. A. G. Hevia, B. Bridier, J. Pérez-Ramírez, Appl. Catal. A 439 (2012) 163-170.
13. B. Bridier, N. López, J. Pérez-Ramírez, Dalton Trans. 39 (2010) 8412-8419.
14. A. Molnár, A. Sárkány, M. Varga, J. Mol. Catal. A 173 (2001) 185-221.
15. H. Lindlar, Helv. Chim. Acta 35 (1952) 446-450.
16. H. Lindlar, R. Dubuis, Org. Synth. 46 (1966) 89.
17. M. P. R. Spee, J. Boersma, M. D. Meijer, M. Q. Slagt, G. van Koten, J. W. J. Geus, Org. Chem. 66 (2001) 1647–1656.
18. A.Yu. Stakheev, P.V. Markov, A.S. Taranenko, G.O. Bragina, G.N. Baeva, O.P. Tkachenko, I.S. Mashkovskii, A.S. Kashin, Kinet. Catal. 56 (2015) 733–740.
19. P. Mäki-Arvela, D. Yu. Murzin, Appl. Catal. A 451 (2013) 251-281.
20. I.S. Mashkovsky, P.V. Markov, G.O. Bragina, G.N. Baeva, A.V. Rassolov, I.A. Yakushev, M.N. Vargaftik, A.Yu. Stakheev, Nanomaterials 8 (2018) 769.
21. S. Furukawa, T. Komatsu, ACS Catal. 7 (2017) 735−765.
22. V.S. Marakatti, S.C. Peter, Prog. Solid State Ch. 52 (2018) 1–30.

23. P.V. Markov, O.V. Turova, I.S. Mashkovsky, A.K. Khudorozhkov, V.I. Bukhtiyarov, A.Yu. Stakheev, Mendeleev Commun. 25 (2015) 367–369.
24. D.Yu. Murzin, J. Mol. Catal. A Chem. 315 (2010) 226–230.
25. D.Yu. Murzin, J. Catal. 276 (2010) 85–91.
26. V.N. Parmon, Doklady Phys. Chem. 413 (2007) 42–48.
27. A.Yu. Stakheev, D.A. Bokarev, I.P. Prosvirin, V.I. Bukhtiyarov in Advanced Nanomaterials for Catalysis and Energy, Elsevier (2019) 295-320.
28. D.Yu. Murzin, Chem Eng Sci 64 (2009) 1046-1052.
29. D.Yu. Murzin, V.N. Parmon, Catal-Spec Period Rep, RSC 23 (2011) 179-203.
30. R. Zanella, C. Louis, S. Giorgio, R. Touroude, J. Catal. 223 (2004) 328-339.
31. M. Haruta, Chem. Rec. 3 (2003) 75-87.
32. G.L. Bezemer, J.H. Bitter, H.P.C.E. Kuipers, H. Oosterbeek, J.E. Holewijn, X. Xu, F. Kapteijn, A.J. van Dillen, K.P. de Jong, J. Am. Chem. Soc. 128 (2006) 3956-3964.
33. V.V. Smirnov, S.A. Nikolaev, G.P. Murav'eva, L.A. Tyurina, A.Yu. Vasil'kov, Kinet. Catal. 48 (2007) 265-270.
34. A.M. Gololobov, I.E. Bekk, G.O. Bragina, V.I. Zaikovskii, A.B. Ayupov, N.S. Telegina, V.I. Bukhtiyarov, A. Yu. Stakheev, Kinet. Catal. 50 (2009) 830-836.
35. I.E. Beck, V.I. Bukhtiyarov, I.Yu. Pakharukov, V.I. Zaikovsky, V.V. Kriventsov, V.N. Parmon, J. Catal. 268 (2009) 60-67.
36. J. Chen, Q. Zhang, Y. Wang and H. Wan, Adv. Synth. Catal. 350 (2008) 453-464.
37. D.Yu. Murzin, Catal. Lett. 142 (2012) 1279-1285.
38. A. Aho, S. Roggan, O. A. Simakova, T. Salmi, D. Yu. Murzin, Catal. Today 241 (2015) 195–199.
39. I.L. Simakova, Yu.S. Demidova, E.V. Murzina, A. Aho, D.Yu. Murzin, Catal. Lett. 146 (2016) 1291–1299.
40. D.A.J.M. Ligthart, R.A. van Santen, E.J.M. Hensen, J. Catal. 280 (2011) 206–220.
41. P.V. Markov, I.S. Mashkovsky, G.O. Bragina, J. Wärnå, E.Yu. Gerasimov, V.I. Bukhtiyarov, A.Yu. Stakheev, D.Yu. Murzin, Chem. Eng. J. 358 (2019) 520-530.
42. S. Furukawa, T. Komatsu, ACS Catal. 6 (2016) 2121-2125.
43. T. Komatsu, K. Takagi, Ken-ichi Ozawa, Catal. Today 164 (2011) 143-147.
44. N.S. Kotsarenko, L.V. Malysheva, I.E. Bekk, V.I. Bukhtiyarov (2010) RF Patent 2387477.
45. S. Ichikawa, H. Poppa, M. Boudart, J. Catal. 91 (1985) 1-10.
46. J.M. Sinfelt, J.L. Carter, D.J.C. Yates, J. Catal. 24 (1972) 283-286.
47. P.V. Markov, G.O. Bragina, G.N. Baeva, O.P. Tkachenko, I.S. Mashkovsky, I.A. Yakushev, N.Yu. Kozitsyna, M.N. Vargaftik, A.Yu. Stakheev, Kinet. Catal. 56 (2015) 601-609.

48. P.A. Ramachandran, R.V. Chaudhari, Three-Phase Catalytic Reactors, Gordon and Breach, New York (1983), p. 32.
49. P. B. Weisz, C. D. Prater, Adv. Catal. 6 (1954) 143–196.
50. I.S. Mashkovsky, P.V. Markov, G.O. Bragina, A.V. Rassolov, G.N. Baeva, A.Yu. Stakheev, Kinet. Catal. 58 (2017) 480-491.
51. I.S. Mashkovsky, P.V. Markov, G.O. Bragina, O.P. Tkachenko, I.A. Yakushev, N.Yu. Kozitsyna, M.N. Vargaftik, A.Yu. Stakheev, Russ. Chem. Bull., Int. Ed. 65 (2016) 425-431.
52. B.M. Choudary, M. Lakshmi Kantam, N. Mahender Reddy, K. Koteswara Rao, Y. Haritha, V. Bhaskar, F. Figueras, A. Tuel, Appl. Catal. A 181 (1999) 139-144.
53. N. Marin-Astorga, G. Alvez-Manoli, P. Reyes, J. Mol. Catal. A: Chem. 226 (2005) 81-88.
54. T.A. Nijhuis, G. van Koten, J.A. Moulijn, Appl. Catal. A 238 (2003) 259–271.
55. S. Dominguez-Dominguez, A. Berenguer-Murcia, A. Linares-Solano, D. Cazorla-Amoros, J. Catal. 257 (2008) 87-95.
56. X.-Y. Quek, Y. Guan, E.J.M. Hensen, Catal. Today 183 (2012) 72–78.
57. P. Tribolet, L. Kiwi-Minsker, Catal. Today 105 (2005) 337-343.
58. N. Semagina, A. Renken, L. Kiwi-Minsker, J. Phys. Chem. C 111 (2007) 13933-13937.
59. P. van Helden, I.M. Ciobîc, R.L.J. Coetzer, Catal. Today 261 (2016) 48–59.
60. H. Bernas, A. Taskinen, J. Wärnå, D.Yu. Murzin, J. Mol. Catal. A. Chem. 306 (2009) 33–39.
61. A. Prestianni, M. Crespo-Quesada, R. Cortese, F. Ferrante, L. Kiwi-Minsker, D. Duca, J. Phys. Chem. C 1186 (2014) 3119-3128.
62. M. Crespo-Quesada, A. Yarulin, M. Jin, Y. Xia, L. Kiwi-Minsker, J. Am. Chem. Soc. 133 (2011) 12787−12794.
63. S. Shaikhutdinov, M. Heemeier, M. Baumer, T. Lear, D. Lennon, R.J. Oldman, S.D. Jackson, H.-J. Freund, J. Catal. 200 (2001) 330–339.
64. B. Nohair, C. Especel, G. Lafaye, P. Marecot, L.C. Hoang, J. Barbier, J. Mol. Catal. A: Chem. 229 (2005) 117–126.
65. M.I. Temkin, Adv. Catal. 28 (1979) 173-291.
66. A.S. Al-Ammar, G. Webb, J. Chem. Soc., Faraday Trans. 1, 75 (1979) 1900-1911.
67. J. Margitfalvi, L. Guczi, A.H. Weiss, React. Kinet. Catal. Lett. 15 (1980) 475-479.
68. S. Leviness, V. Nair, A.H. Weiss, Z. Schay, L. Guczi, J. Mol. Catal. 25 (1984) 131-140.
69. D.Yu. Murzin, Catal. Lett. 145 (2015) 1948–1954.
70. R. van Hardeveld, F. Hartog, Surf. Sci. 15 (1969) 189-230.
71. H. Haario Modest 6.0-A User's Guide. ProfMath, Helsinki (2001).

72. D.Yu. Murzin, T. Salmi, Catalytic Kinetics, Elsevier, 2016.
73. H. Haario, E. Saksman, J. Tamminen, Bernoulli 7 (2001) 223–242.